THE UNIVERSITY OF MICHIGAN

COLLEGE OF ENGINEERING
Department of Electrical Engineering
Space Physics Research Laboratory

Technical Report

AN EJECTABLE NOSETIP FOR SOUNDING ROCKET EXPERIMENTS

Prepared by

P. O. Handy
D. J. Beechler
D. B. Jones

ORA Project 036320

under contract with:

NATIONAL AERONAUTICS AND SPACE ADMINISTRATION
GODDARD SPACE FLIGHT CENTER
CONTRACT NO. NAS5-21147
GREENBELT, MARYLAND

administered through:

OFFICE OF RESEARCH ADMINISTRATION ANN ARBOR

July 1971

TABLE OF CONTENTS

LIST OF ILLUSTRATIONS

LIST OF ILLUSTRATIONS (Concluded)

1. INTRODUCTION

The present report describes an ejectable nosetip for a sounding rocket payload. The primary purpose of the nosetip is to vacuum seal the radioactive ionization gauge (Handy, 1970) in a payload from undesirable contamination effects until the required ejection time (altitude) during rocket flight. Nosetip ejection is required at altitudes of 30 to 35 km so that the upleg rocket payload measurement, from which the neutral properties of the atmosphere are deduced (Cittadini, 1970), will just overlap high altitude balloon radiosonde measurements. At these altitudes and sounding rocket velocities, aerodynamic pressure is appreciable.

The ejectable nosetip is designed to be aerodynamically unstable so that upon ejection, the nosetip pitches and tumbles, encountering lift and drag forces which move the nosetip to one side and downward relative to the payload, thus assuring a previously undisturbed atmosphere for upleg measurements taken by the payload.

To date, fourteen sounding rocket experiments with ejectable nosetips of this design have been launched. Each of the nosetips was ejected successfully at a predetermined time (altitude) during flight. Data from the rocket experiments also indicated that each ejected nosetip pitched and tumbled past the rocket at distances predicted.

Since this nosetip is not dependent on a payload for any support functions, it could possibly find application on other sounding rocket experiments as a heat shield, a frontal sealing device, or as a means of obtaining a lower drag configuration for ejection altitudes up to 55 km. Above approximately 55 km, aerodynamic effects become vanishingly small and the nosetip is not likely to pitch and tumble any significant distance from the rocket flight path.

The mechanical ejection scheme, most of the design considerations, and the actuator time delay firing circuit for the nosetip are presented herein. Also included are trajectories of a nosetip ejected from a payload, calculated for various initial conditions.

2. GENERAL DESCRIPTION

The external configuration of the nosetip is a 9 deg half-angle cone having a base skirt diameter of 4.250 in. Because significant aerodynamic heating is experienced during rocket flight, the outer shroud or wall of the nosetip is machined from 303 stainless steel. Most of the internal structure is fabricated from 2024-T351 aluminum because it is easily machined. Figure 1 is a machine assembly drawing of the nosetip.

In assembly stages, before final integration, the nosetip is divided into three basic sections or subassemblies. These are a base sealing subassembly, an actuator and electronics subassembly, and a forward shroud. The three subassemblies are shown in Figure 2.

The basic mechanism for locking the nosetip to a keyed payload and a seal plate section comprises the base sealing subassembly. This subassembly can be installed and locked on a payload in a suitable environment and then vacuum attended to at any time prior to installation of the electronics package.

The pyrotechnic and electronics package, which is mated to or, if necessary, easily removed from the base sealing section, is comprised of a dual bridge sealed piston actuator, pressure switches, batteries, and electronic time delay firing circuitry. The piston actuator provides the sole means of release activation and ejection of the nosetip from a payload. For redundancy, two time delay firing circuits are employed. Pressure switches in a series mode are used to isolate the firing circuits from the actuator until after launch, thus satisfying range safety requirements.

Thermal shielding attached to the inside wall of the forward shroud provides the necessary thermal insulation for the electronics package. Mounted last, the forward shroud completes the final assembly of a nosetip.

The internal structure and components are fabricated and arranged such that approximate weight symmetry about the cone axis is achieved. A complete nosetip is 13 in. long and weighs approximately 3.4 lb. A completely assembled nosetip is shown in Figure 3 and a nosetip mated to a sounding rocket experiment is shown in Figure 4.

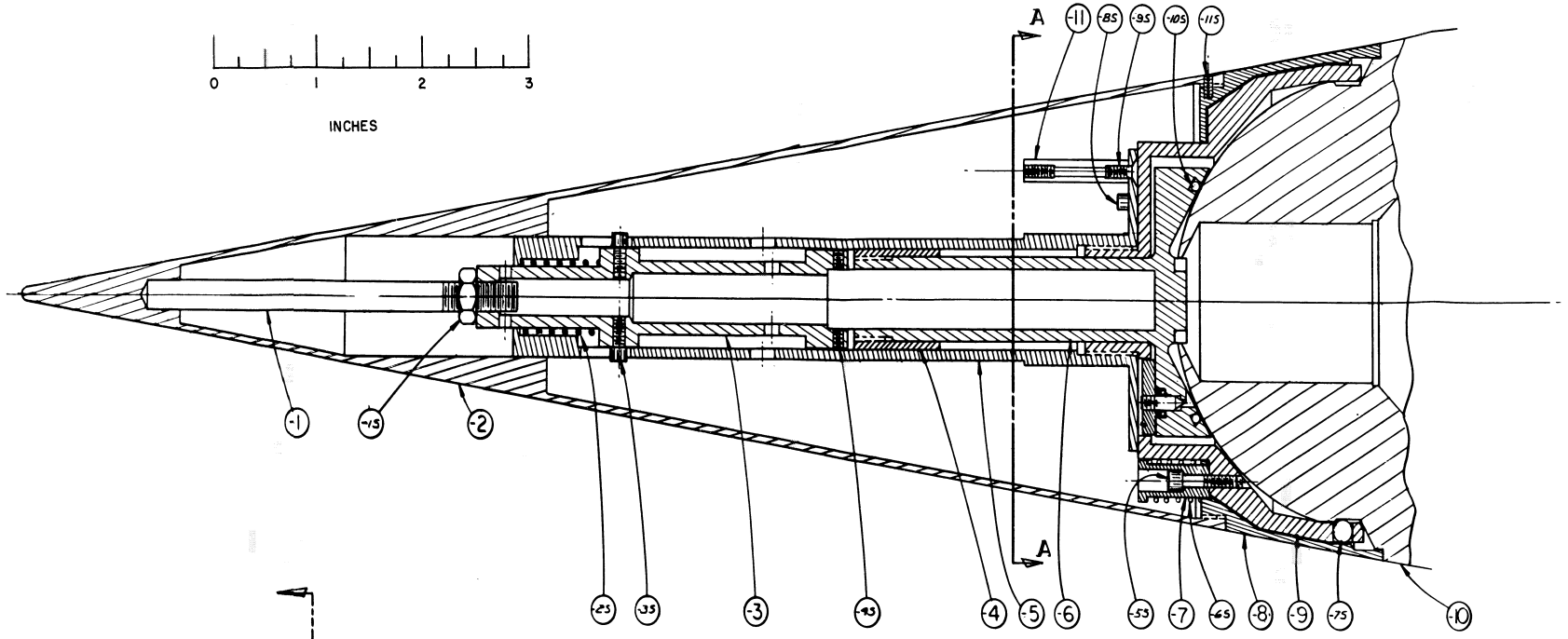

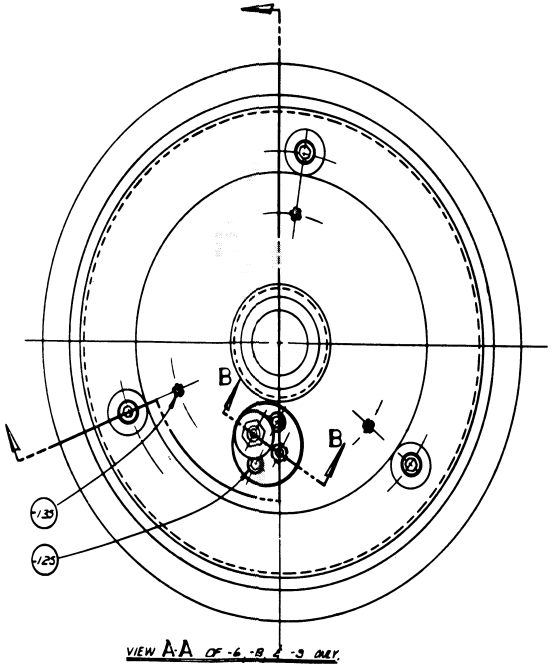

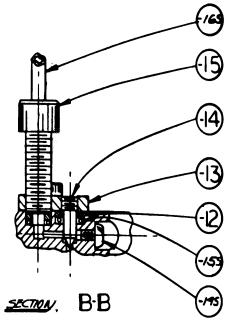

1			-165	PUMP DOWN LINE	1/8 O.D. TUBE		
2		PACKED W/ E-6	-155	O-RING			
1			-145	SEAL SCR.	#4-40 UNC x .125		STN. STL.
3		JAM SCR.	-135	SOC. HD. SET SCR.	#4-40 UNC x .125		STL.
2			-125	SOC. HD. CAP SCR.	#2-56 UNC x .125		STL.
2		LOCK	-115	SOC. HD. SET SCR	#2-56 UNC x .187		STL.
1		PACKED W/ E-132	-105	O-RING			SILICA N.
2			-95	FLT. HD. SOC. SCR	#4-40 UNC x .25		STL.
1		LOCK	-85	SOC. HD. CAP SCR	#4-40 UNC x .187		STL.
3		DETROIT BALL	-75	BALL	.187 DIA		STL.
3		ASSEMBLED IN C-368 OUT-1500	-65	SPRING			STL.
3			-55	SOC. HD. CAP SCR	#4-40 UNC x .500		STL.
2			-45	SOC. HD. SET. SCR.	#4-40 UNC x .187		STL.
2			-35	SOC. HD. CAP SCR	#4-40 UNC x .187		STL.
1		ASSEMBLED IN C-368 OUT-1500	-25	SPRING			STL.
2			-15	HEX. NUT JAM.	1/4-28 NF		STL.
1		A-022-029-2	-15	JAM SCR.			
1		A-022-029-1	-14	STEM			
1		A-022-028	-13	VALVE COVER			
2		A-022-029-3	-12	WASHER			
2		A-022-080	-11	SPACER			
1		D-022-030	-10	TIP SECTION			REF
1		C-022-026	-9	BALL RETAINER			
1		C-022-022	-8	LOWER SHROUD			
3		A-022-027	-7	SPRING RETAINER			
1		C-022-019	-6	PLUNGER			
1		C-022-021	-5	SLEEVE			
1		A-022-024	-4	STOP			
1		B-022-025	-3	BOLT			
1		D-022-023	-2	UPPER SHIELD			
1		A-022-020	-1	THREADED ROD			
L.H. R.H. NO. REQ'D.		PART NO.	L.H. R.H. DASH NO.	NAME	SIZE		DESCRIPTION MATERIAL

Figure 1. Assembly drawing of the nosetip.

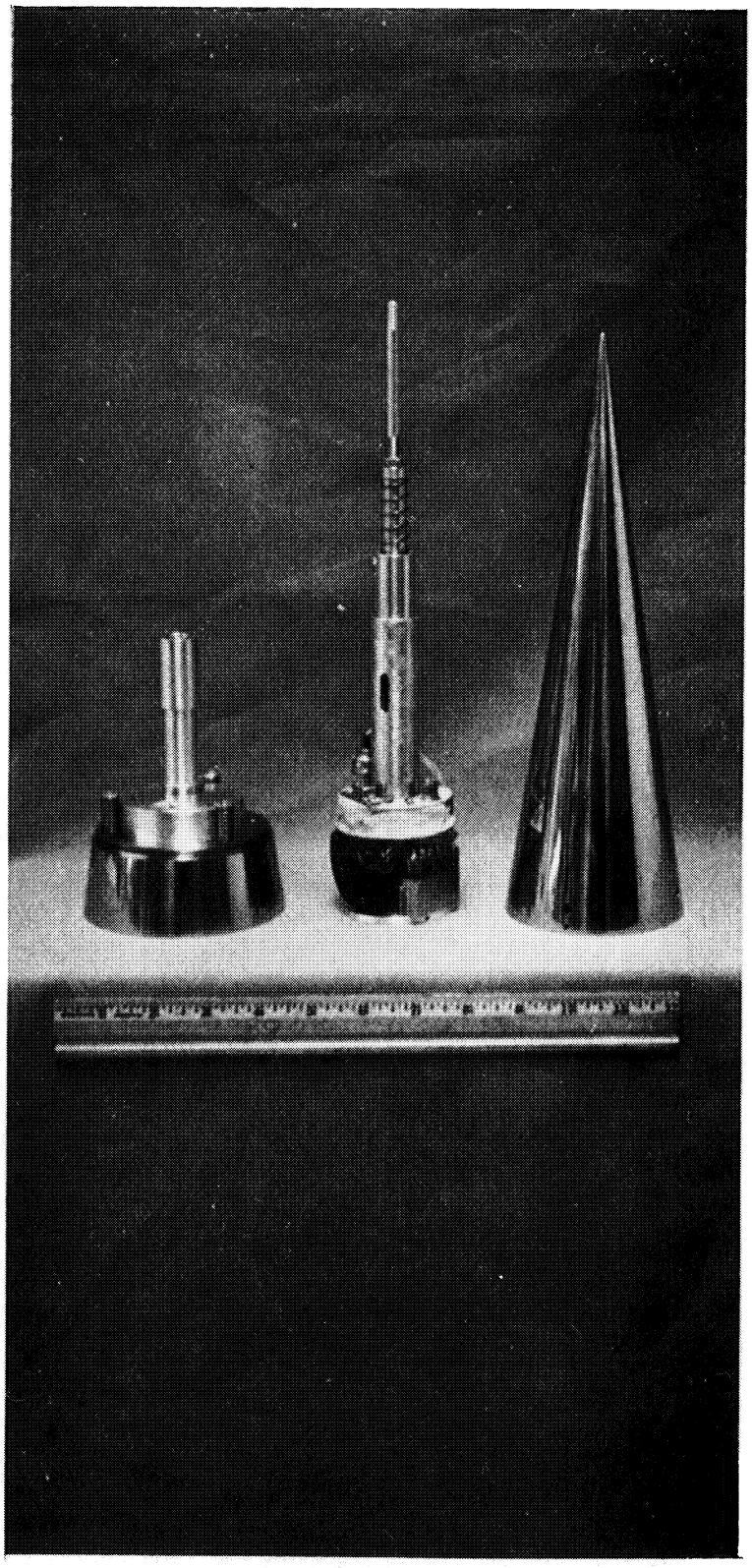

Figure 2. Nosetip subassemblies.

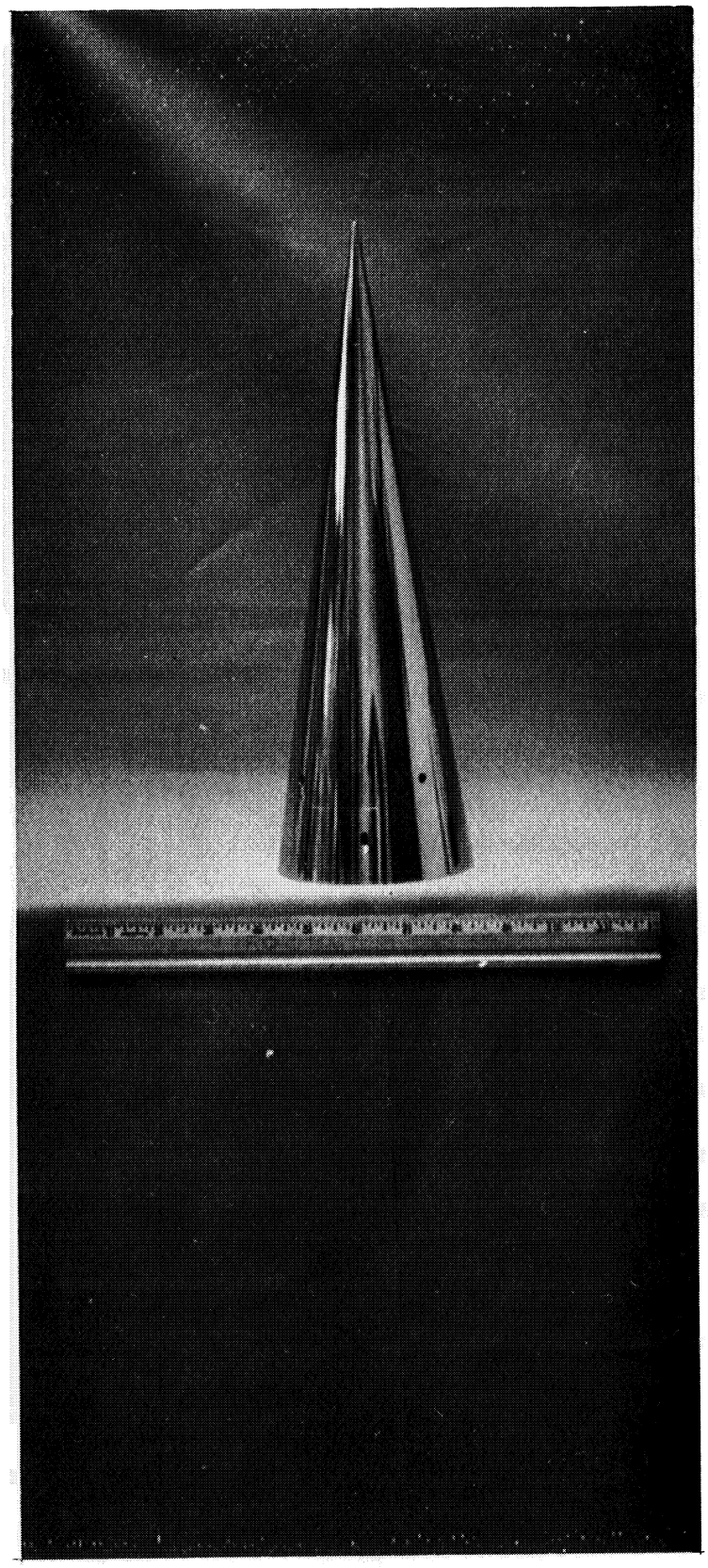

Figure 3. Assembled nosetip.

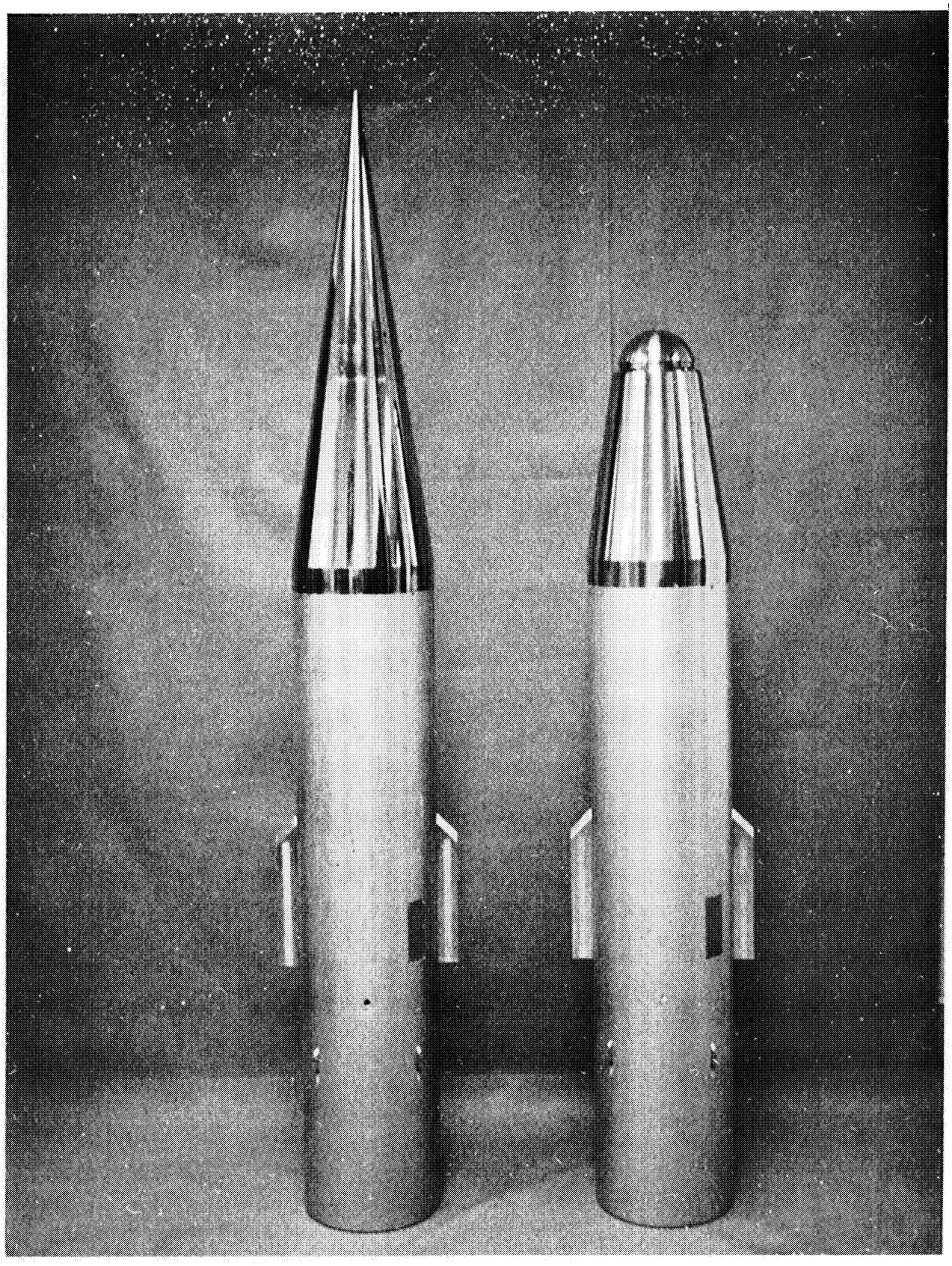

Figure 4. Ejectable nosetip mated to a sounding rocket payload.

3. MECHANICAL DESIGN CONSIDERATIONS

Since low angles of attack during payload measurement are desired, one of the first design considerations was to minimize any upsetting moments imparted to a rocket payload system by the ejection of a nosetip. Consequently, straightforward unlocking and ejection of the nosetip from a payload is employed. With this scheme, moments created during the ejection sequence are small and have little effect on rocket stability even at altitudes where aerodynamic restoring forces would otherwise be ineffective.

The locking and ejection scheme can perhaps be easily understood by referring to the series of views shown in Figure 5, which illustrates the unlocking sequence. For the sake of clarity some of the drawing details (thread joints, etc.) have been deliberately left out. The first view shows the nosetip locked in position to a keyed payload. The sequence of unlocking events is as follows:

(a) Upon firing, the piston of the actuator is forced against the seal plate moving the pushrod (view 2) and outer shroud forward. The six balls captured to provide locking are then released as shown in view 3.

(b) The parts (outer shroud, pushrod, etc.) shown in view 2 continue to move forward, shouldering at "B" (view 4). The section on which the electronics package is mounted then moves forward with the outer shroud, pushrod, etc.

(c) As the complete nosetip assembly (less seal plate) moves forward, the seal plate is then lifted from the payload by the shouldering at "C" (view 4).

(d) The complete assembly as a whole then continues to move forward from the payload, completing the ejection sequence.

In a locked position, three springs (6s, Figure 1) force the outer shroud of the nosetip against the payload at "A" (view 1, Figure 5), which keeps the six balls captured, maintaining the locked position. For pressure relief and for proper baro-switch function four small holes are drilled in the cone wall, which results in the inside pressure being equal to the outside cone wall pressure. Consequently, the three springs must withstand the outer shroud deceleration force during the high drag phase of rocket flight occurring just after booster and second stage burnouts. In their compressed state, the three springs provide a force of 27 lb, which more than offsets the maximum deceleration force of 10 lb during rocket flight.

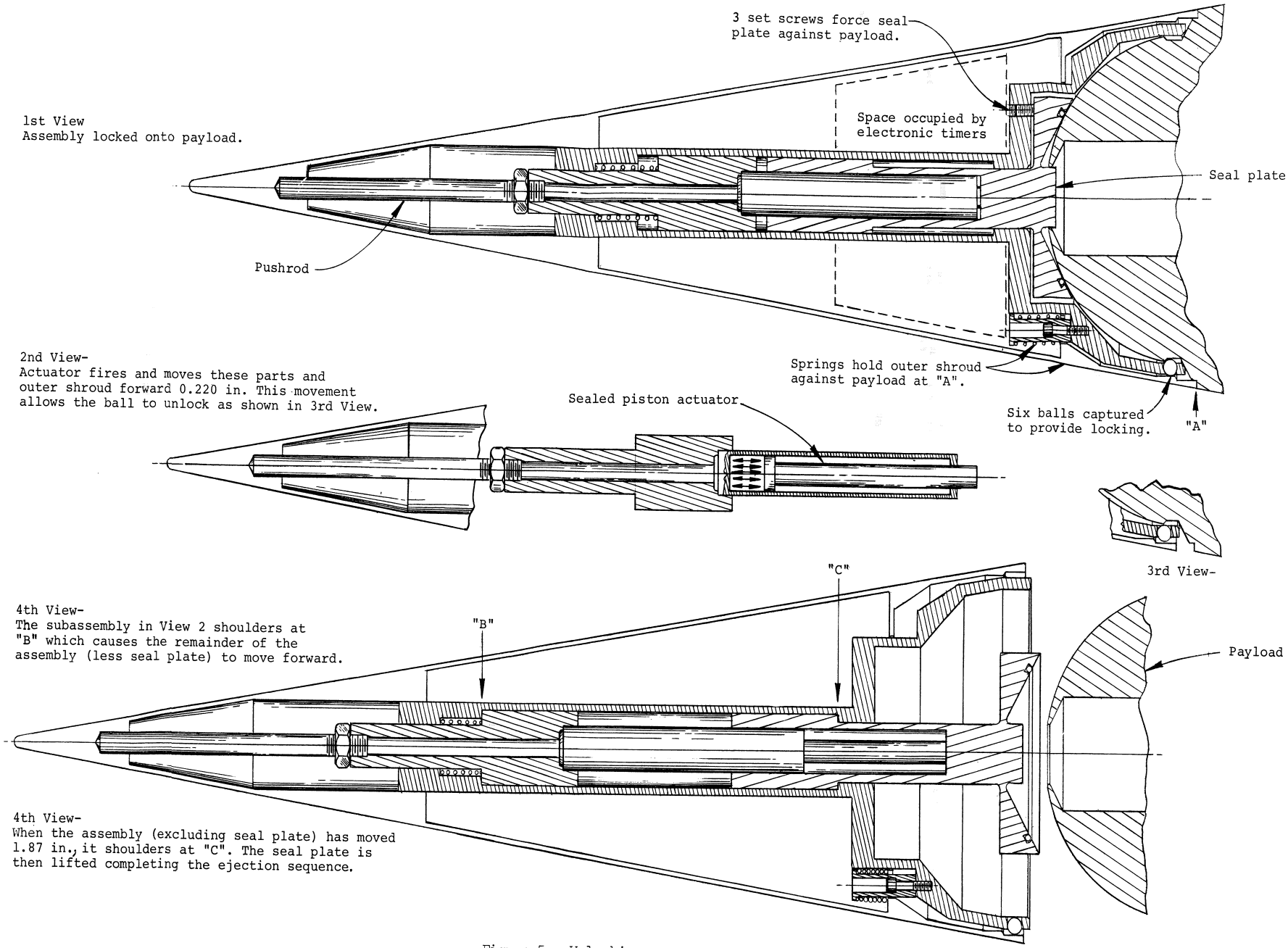

Figure 5. Unlocking sequence.

With the type of lock mechanism employed, thermal expansion effects due to aerodynamic heating are easily accommodated so that the nosetip neither locks up mechanically nor seizes to the payload. In the axial direction, the outer shroud is designed to expand freely away from the pushrod a distance of 0.050 in., much less than the 0.220 in. allowed before difficulty in the ejection sequence occurs. Structural expansion in the radial direction poses no problem because the anticipated temperatures increase the base skirt diameter approximately 0.008 in. in the direction opposite to that which would possibly cause the nosetip to seize to a payload during flight. As a check on these design considerations an ejection test at elevated temperature was performed at the Goddard Space Flight Center facilities. The test setup and results are described in Appendix C.2.

In the resulting motion of an ejected nosetip both the center of mass location and the initial conditions are of primary importance. Upon ejection the center of mass is established in its predetermined position by a residual force of approximately 75 lb exerted by the piston actuator which maintains the nosetip in an extended configuration (view 4, Figure 5). Initial straightforward ejection of the symmetric nosetip within predictable limits is accomplished by utilizing the seal plate as a stable platform for pushoff upon actuator firing.

As mentioned previously, the primary purpose of a nosetip is to vacuum seal the radioactive ionization gauge in a payload. This is accomplished by a seal plate (Figure 6) which is forced against the payload by three setscrews (-13s, Figure 1) compressing an "O" ring seal. The seal plate is fabricated such that a pumpdown line from a vacuum system can be easily attached and removed later by a knurled jam screw. Seal-off after pumpdown is accomplished by utilizing a small needle valve. A view of the base sealing subassembly which includes the seal plate section with pumpdown line attached is shown in Figure 7.

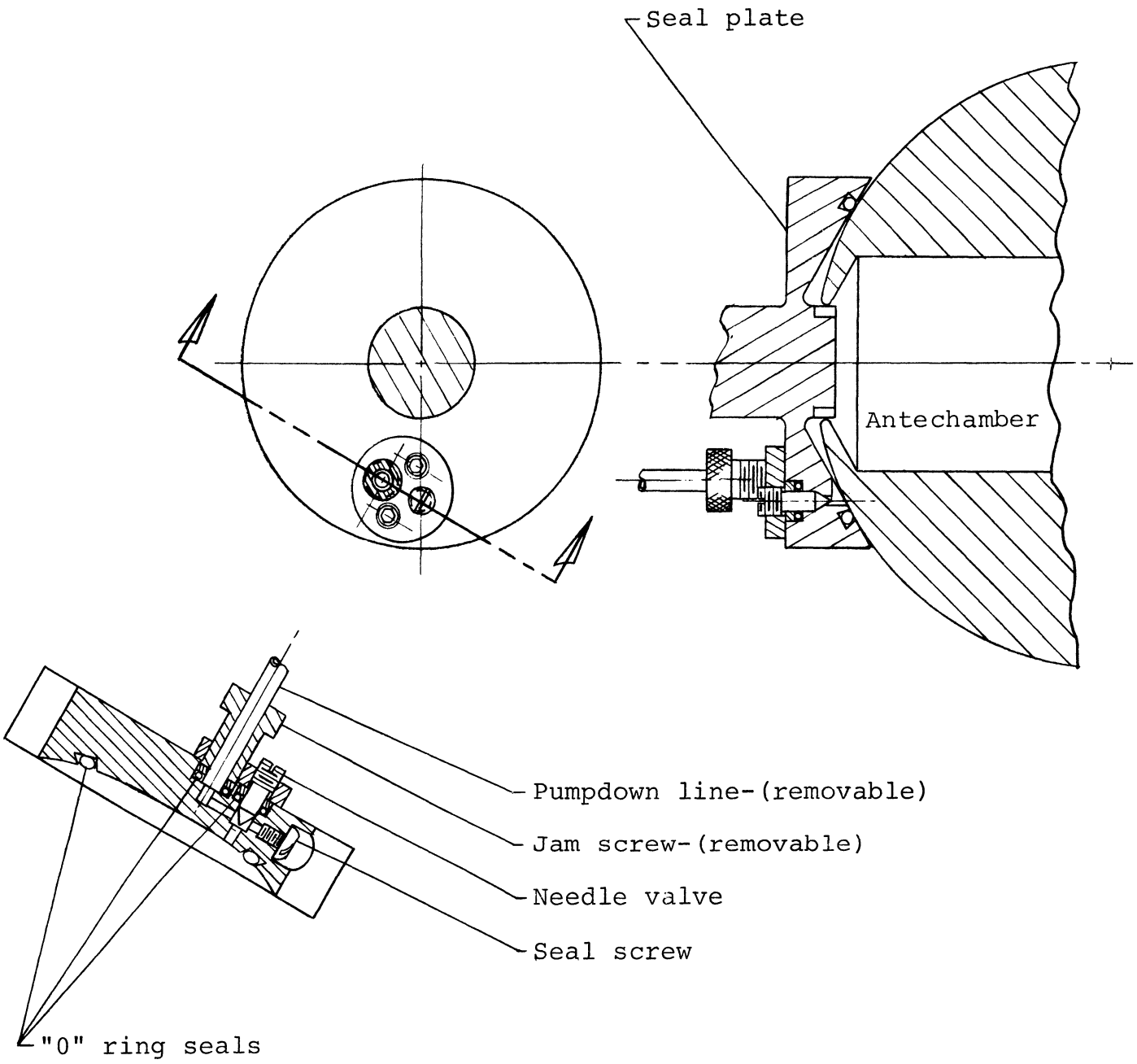

Figure 6. Seal plate section.

Figure 7. Base sealing subassembly with pumpdown line attached.

4. ACTUATOR FIRING SCHEME

For actuator firing at a predetermined time (altitude) during rocket flight, only two different techniques, to date, have been used. A schematic of the electronic circuit which was used successfully in the first two ejectable nosetips is shown in Figure 8. In this scheme pressure switches provide the logic function for actuator firing. Since nosetip ejection was to occur at low pressure where pressure switch accuracy is unobtainable, a simple circuit was employed to delay actuator firing from the time of accurate pressure switch function to the required ejection time during rocket flight. For firing redundancy, two identical but completely separate circuits to the dual bridge actuator were used. Two pressure switches in series with each of the two electronic circuits were necessary in order to satisfy range safety requirements.

The second scheme, which has been employed in nosetips subsequent to the first two, uses the first motion of a rocket on the launcher as a logic function. The circuit schematic is shown in Figure 9. Again, two electronic time delay firing circuits are employed. The two microswitches which initiate the electronic timers are operated by a mechanical pullaway. In this scheme the delay time is set directly to the required flight time for nosetip ejection. The two pressure switches in series with the ignitors serve only to satisfy range safety requirements.

A view of the actuator and electronics subassembly is shown in Figure 10. Also shown are HR.01 wet cells manufactured by Yardney Electronics Corporation and used for the battery supplies, model ES4-20 pressure switches manufactured by Carmac Company, and two piston actuators (one having been fired) manufactured by Atlas Chemical Industries Incorporated. Because an actuator has not been installed in the subassembly, the pushrod section (1, 3 in Figure 1) is not shown in its proper location.

Shielding the electronics from the effects of aerodynamic heating was easily accomplished by spacing a 0.005 in. steel sheet insert approximately 0.040 in. from the cone wall so that direct thermal contact between the two did not occur. Two complete wraps of aluminum foil and armalon around the electronics provided additional multiple reflecting surfaces and low heat conduction paths, thus providing more insulation than necessary to delay the heating effects even beyond the time of nosetip ejection. The steel sheet insert and the wrapping insulation are shown in Figure 11 next to the forward shroud.

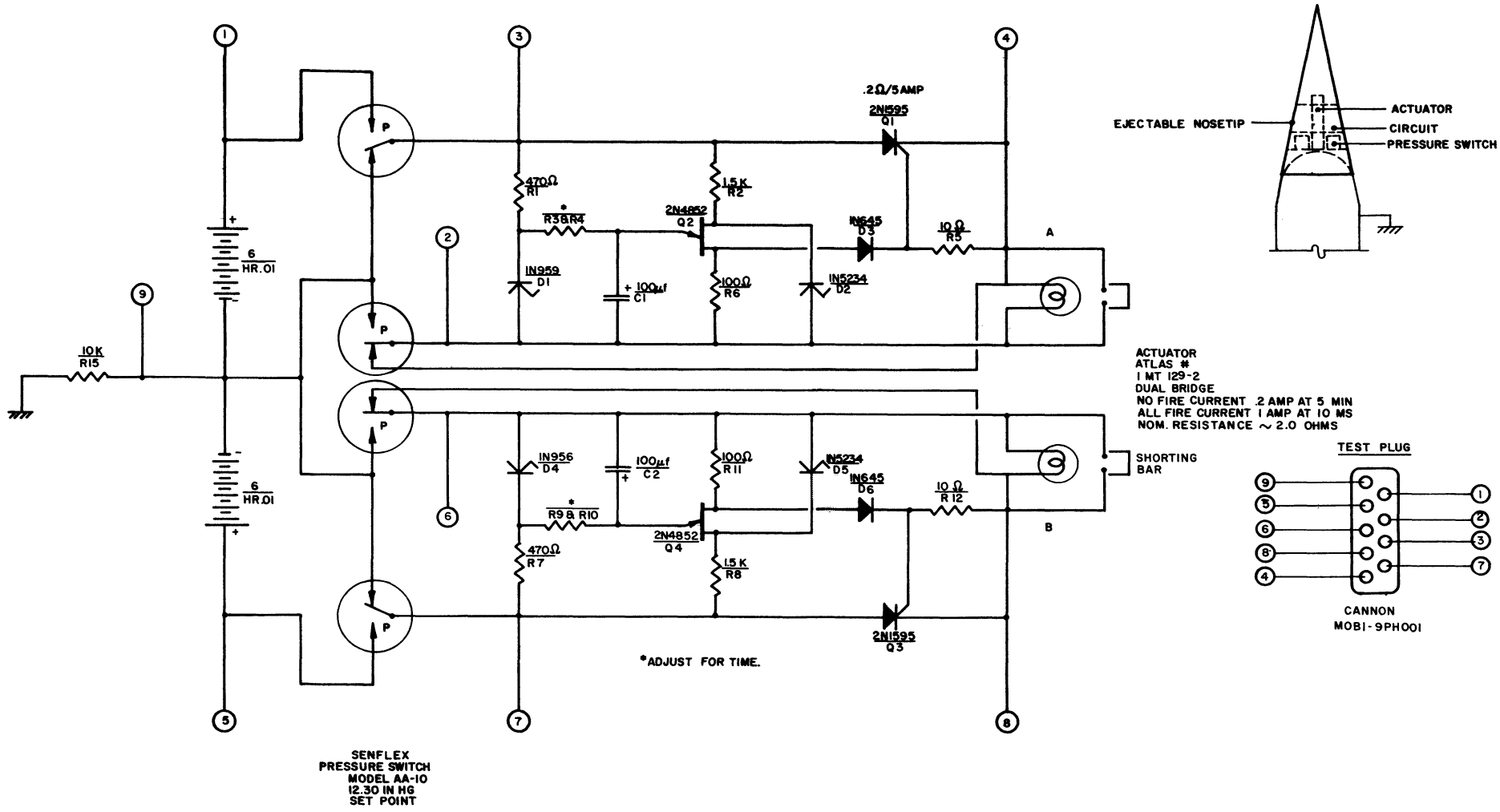

Figure 8. Timer and actuator firing circuit.

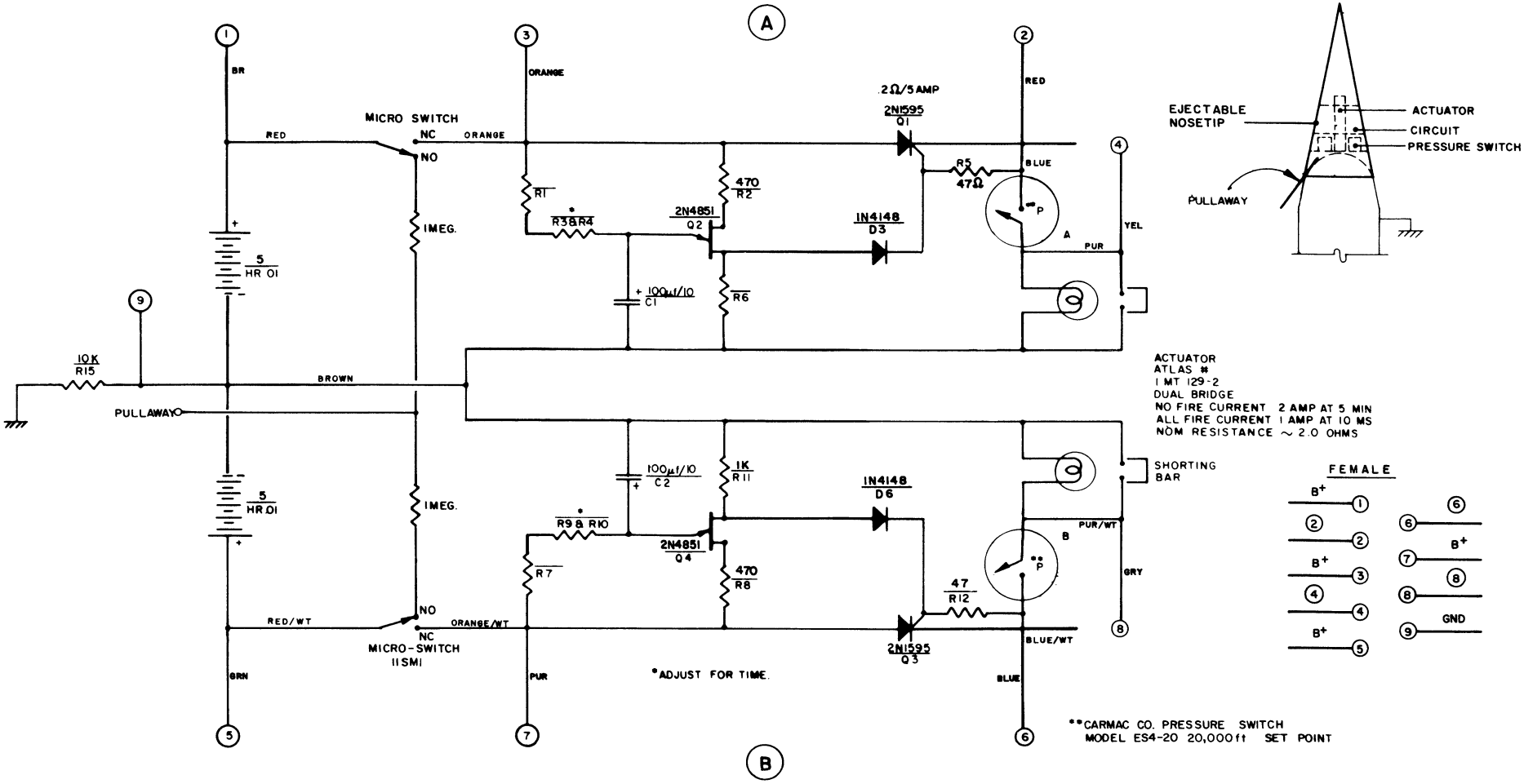

Figure 9. Timer and actuator firing circuit, Model E.

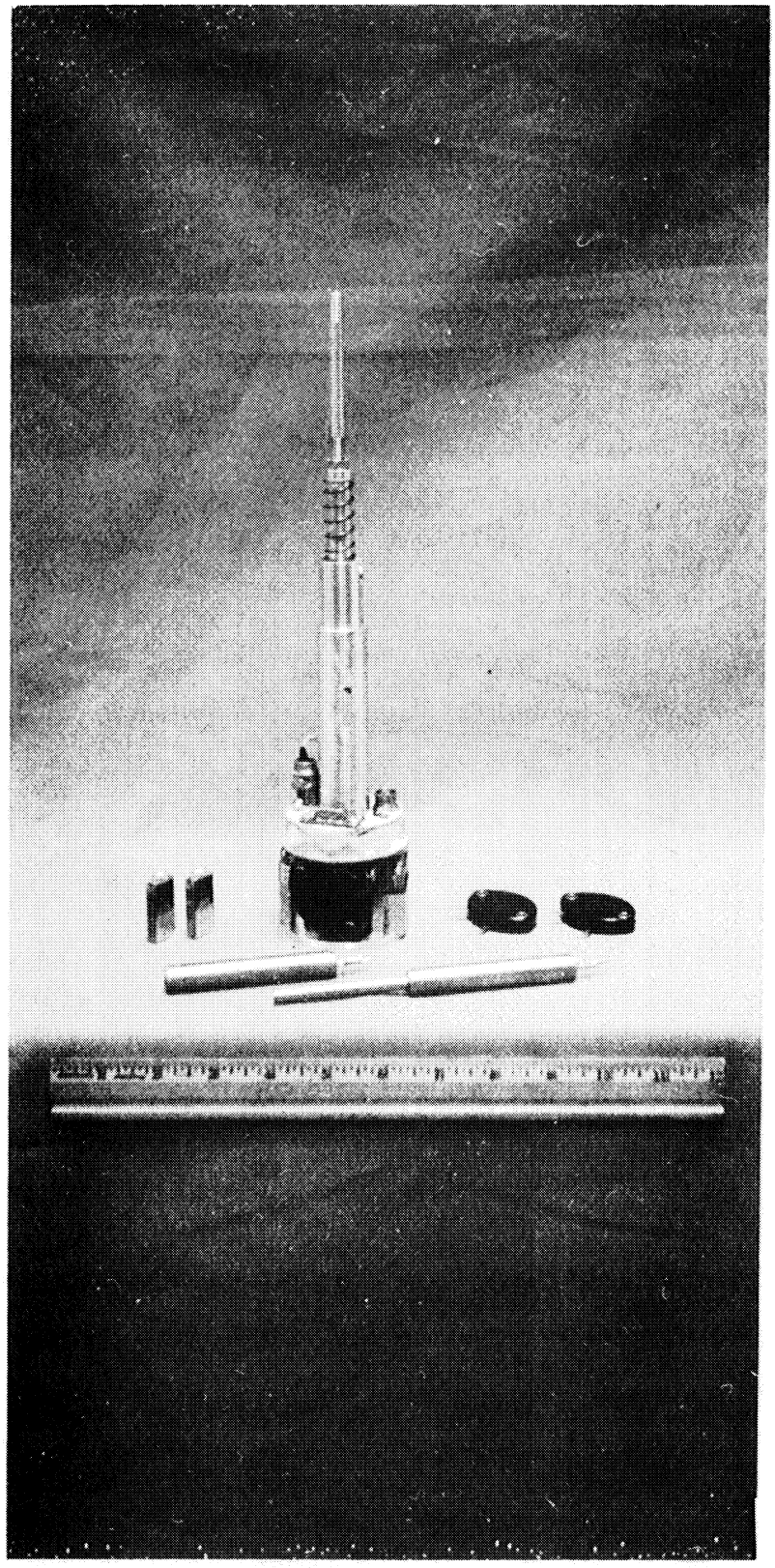

Figure 10. Actuator and electronics subassembly.

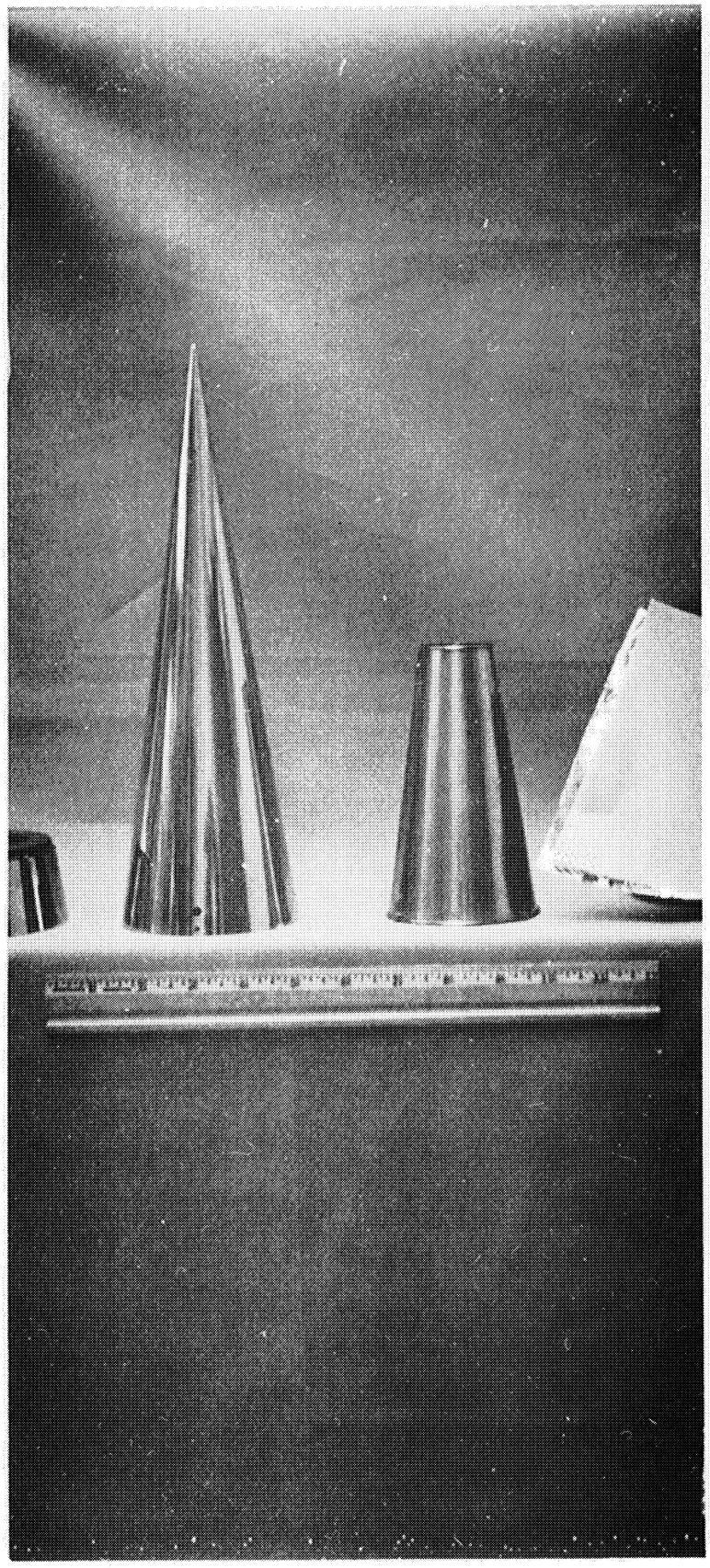

Figure 11. Forward shroud and thermal insulation.

5. EJECTED NOSETIP TRAJECTORIES

5.1 DETAILED TRAJECTORY RESULTS

The equations of motion developed in Appendix A which predict the motion and path and an ejected nosetip relative to the payload are summarized below.

$$I_{xx}\frac{d^2\alpha}{dt^2} + I_{zz}\left(\frac{d\beta}{dt}\cos\alpha + \omega\right)\frac{d\beta}{dt}\sin\alpha - I_{xx}\left(\frac{d\beta}{dt}\right)^2\sin\alpha\cos\alpha$$

$$= (1.150 + C_M/C_N - \bar{x})C_N q_{\infty_i} SDe^{-t/t_1}$$

$$I_{xx}\frac{d^2\beta}{dt^2}\sin\alpha + 2I_{xx}\frac{d\beta}{dt}\frac{d\alpha}{dt}\cos\alpha - I_{zz}\left(\frac{d\beta}{dt}\cos\alpha + \omega\right)\frac{d\alpha}{dt} = 0$$

$$I_{zz}\frac{d}{dt}\left(\frac{d\beta}{dt}\cos\alpha + \omega\right) = 0$$

$$\frac{d^2x_o}{dt^2} = (C_N\cos\alpha - C_A\sin\alpha)\frac{q_{\infty i}S}{m}e^{-t/t_1}\sin\beta$$

$$\frac{d^2y_o}{dt^2} = (C_A\sin\alpha - C_N\cos\alpha)\frac{q_{\infty i}S}{m}e^{-t/t_1}\cos\beta$$

$$\frac{d^2z_o}{dt^2} = D_i e^{-t/t_2} - (C_N\sin\alpha + C_A\cos\alpha)\frac{q_{\infty i}S}{m}e^{-t/t_1}.$$

These equations were solved by computer for a number of initial conditions and parameter values. Figures 12, 13, 14, and 15 illustrate the effects some of the more important of these parameters have on the resulting trajectory solutions. For reference, the path labeled 1 in each of these figures was computed using the measurement values from Appendices B and C.1 and for nosetip ejection at an altitude of approximately 36 km with an initial angle of attack of 1 deg.

One of the important parameters to which the motion and path of an ejected nosetip is very sensitive is the center of mass location. With all other parameter values the same, a center of mass change from $\bar{x}$ = 0.929 to 0.882 (i.e., a 0.2 in. location change for this design) decreases the radial distance which the nosetip pitches and tumbles past the rocket payload by approximately one third. The detailed computation results which illustrate this effect are shown in Figure 12.

The effect of varying the initial separation or ejection velocity of the nosetip from the payload by 7 ft/sec is shown in Figure 13. This effect is not large. The 7 ft/sec velocity variation is certainly considered an outside limit for this design because the Atlas piston actuator employed for release activation has been observed, from the ground based ejection tests (Appendix C.1), to be a consistent performer.

The trajectories for nosetip ejection at altitudes of 28, 36, and 42 km are shown in Figure 14. The variation between each of these is quite large and is due to the rapid decrease in free-stream aerodynamic pressure with increasing altitude. The trajectories for ejection at altitudes of 28 and 36 km are shown so as to bracket the original design ejection altitude of 30 to 35 km.

One of the problems with attempting to predict the motion of an ejected nosetip is that the initial angular conditions (i.e., initial angle of attack, initial tumble rate, etc.) are not known prior to nosetip ejection. However, from the results of ejection tests described in Appendix C, the initial rotation rates are believed to be small, and thus for this problem are set equal to zero. The initial angle of attack remains unknown and is due to the normally occurring attitude variations encountered by the rocket vehicle during flight, which in the altitude region of interest is usually less than 3 deg. Thus nosetip trajectories were determined for initial angles of attack of 0.1 deg, 1 deg, and 10 deg. The results are shown in Figure 15.

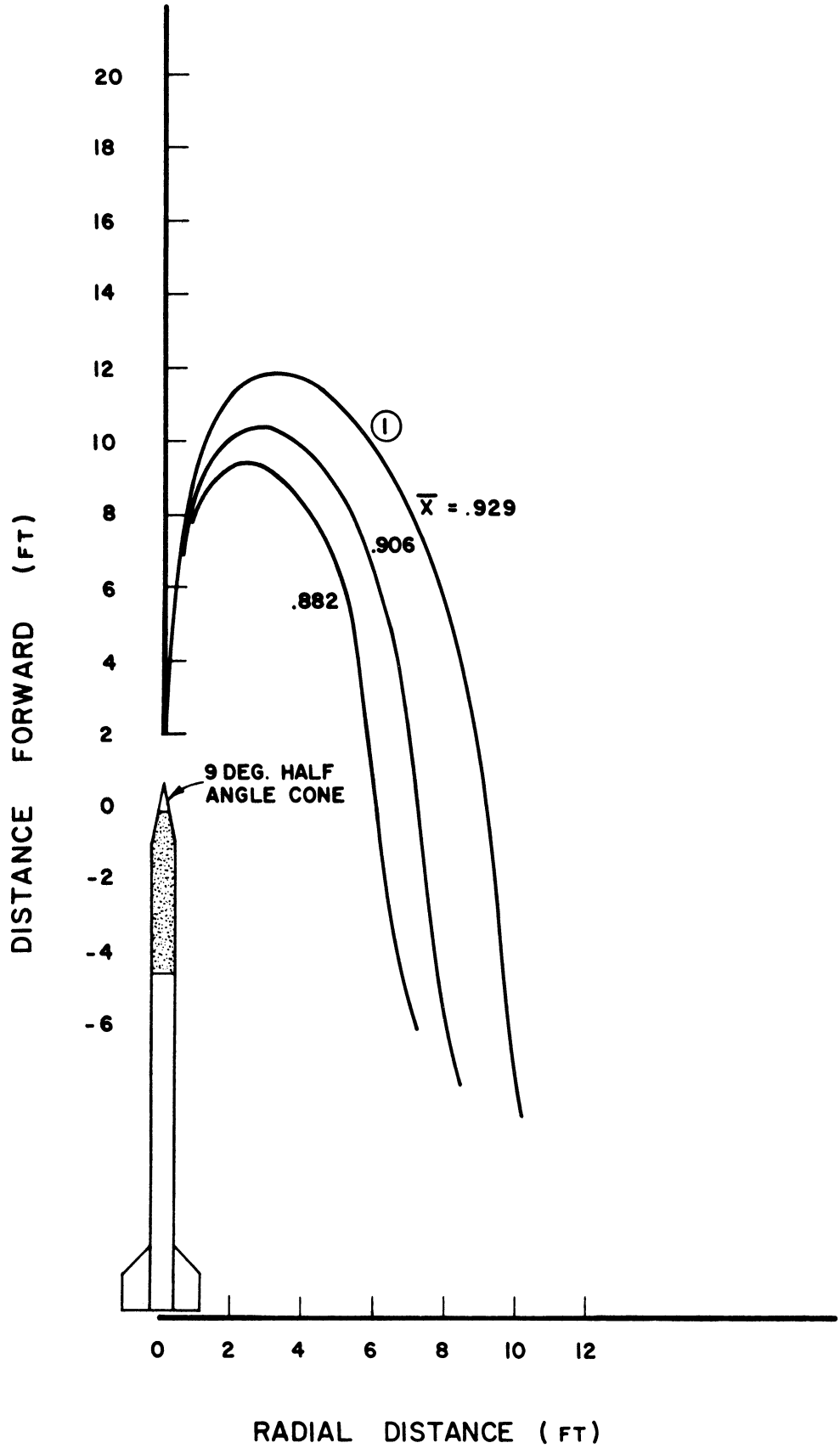

Figure 12. Effect of varying the center of mass location.

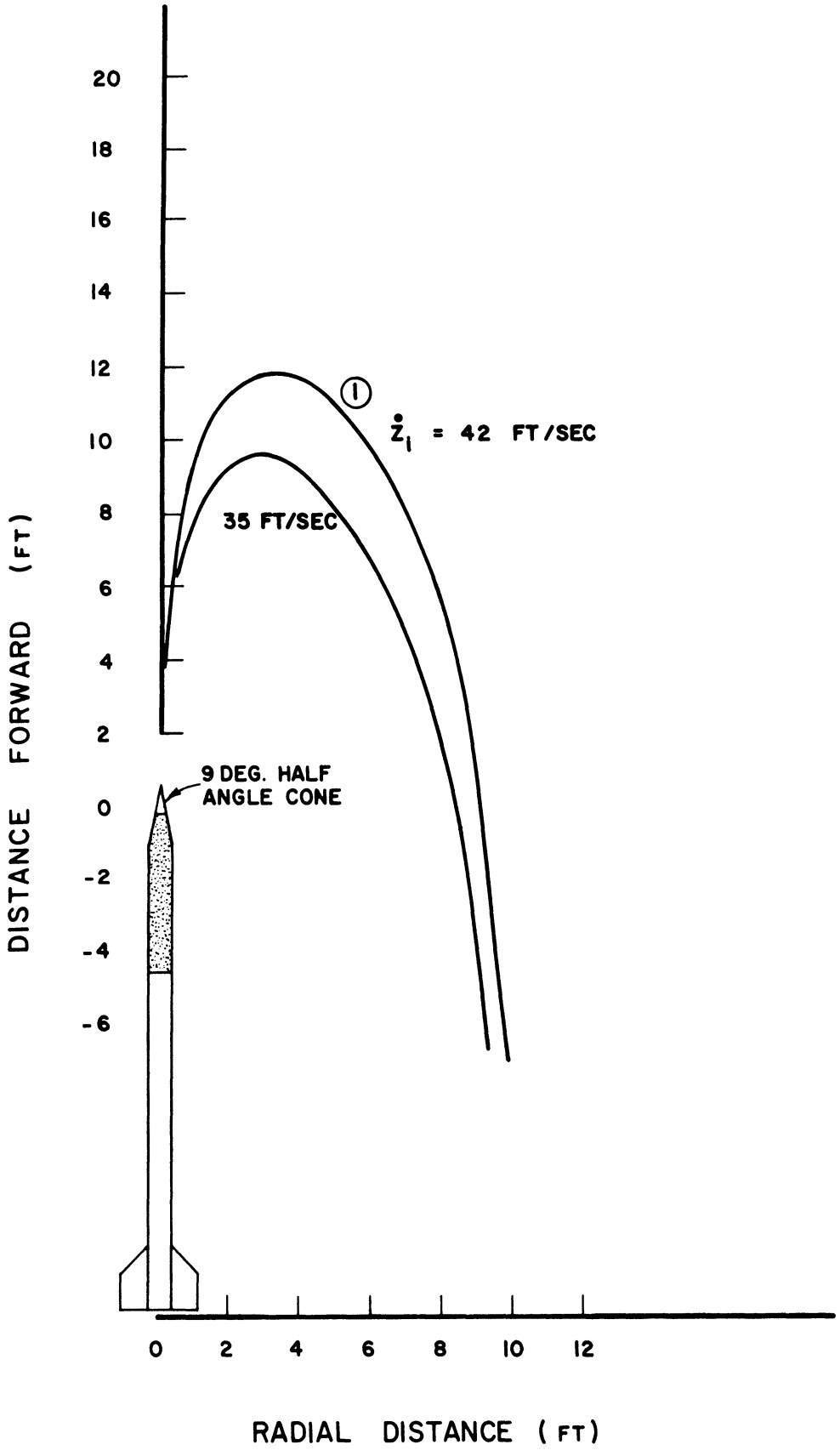

Figure 13. Effect of varying the initial separation velocity.

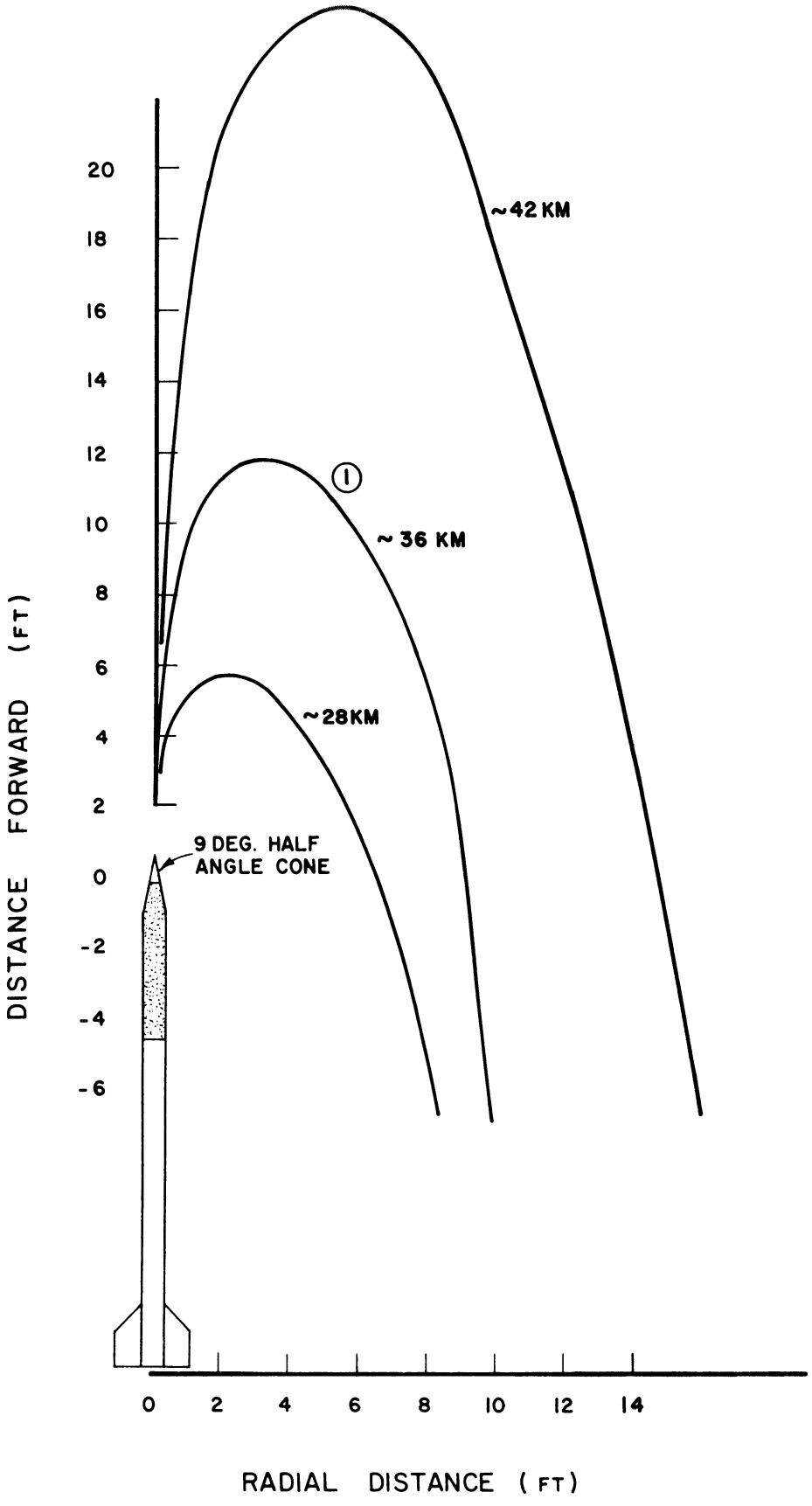

Figure 14. Trajectories for nosetip ejection at 28, 36, and 42 km.

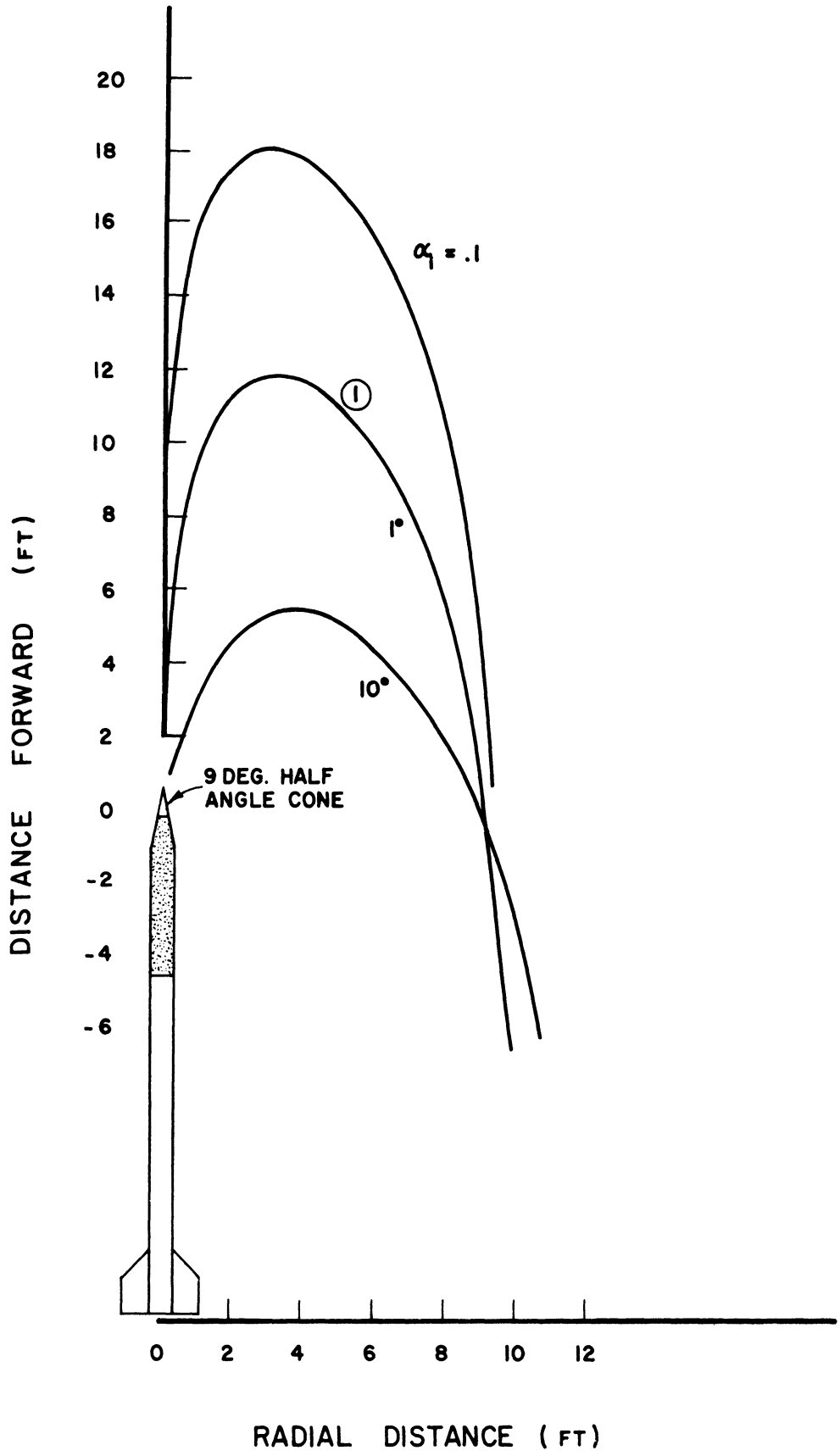

Figure 15. Trajectories for nosetip ejection with initial angles of attack of 0.1, 1, and 10 deg.

~~Figure 16.~~

5.2 PERFORMANCE CHART

The equations of motion, written above, were cast in nondimensional form with the parameters organized into significant groups (Handy, 1971). The results of the computer solution are shown in Figure 17 which is a plot of the nondimensional variable Z_{max} versus the nondimensional variable $R_{z=0}$ for three different initial angles of attack and various values of W and $\dot{Z}_i$ where

$$Z_{max} = \frac{(1-\bar{x})}{\alpha_i} \left(\frac{mD}{I_{xx}}\right) \cdot z_{max},$$

$$R_{z=0} = W \cdot (1-\bar{x})\left(\frac{mD}{I_{xx}}\right) \cdot r_{z=0},$$

$$\dot{Z}_i = \frac{(1-\bar{x})\left(\frac{mD}{I_{xx}}\right) \dot{z}_i}{\left[\left(\frac{q_{\infty i} S}{mg}\right)(1-\bar{x})\left(\frac{mD}{I_{xx}}\right)g\right]^{1/2}},$$

$$W = \frac{(I_{zz}\omega_i/I_{xx})}{(1-\bar{x})\left(\frac{mD}{I_{xx}}\right)\dot{z}_i}.$$

Only the two points Z_{max} and $R_{z=0}$ on the nosetip's path, as shown in Figure 16, can be obtained from Figure 17. However, the importance of any parameter is easily evaluated. In general, for values of H>1 where

$$H = \frac{(I_{zz}\omega_i/I_{xx})}{\left[\left(\frac{q_{\infty i} S}{mg}\right)(1-\bar{x})\left(\frac{mD}{I_{xx}}\right)g\right]^{1/2}},$$

it was found that the nosetip did not spin and pitch unstably any significant distance from the rocket flight path.

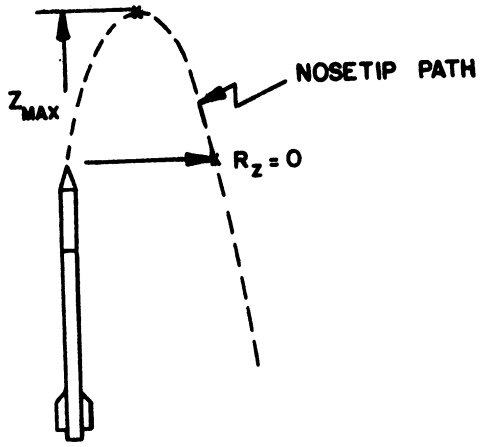

Figure 16. Definition of Z_{max} and $R_{Z=0}$.

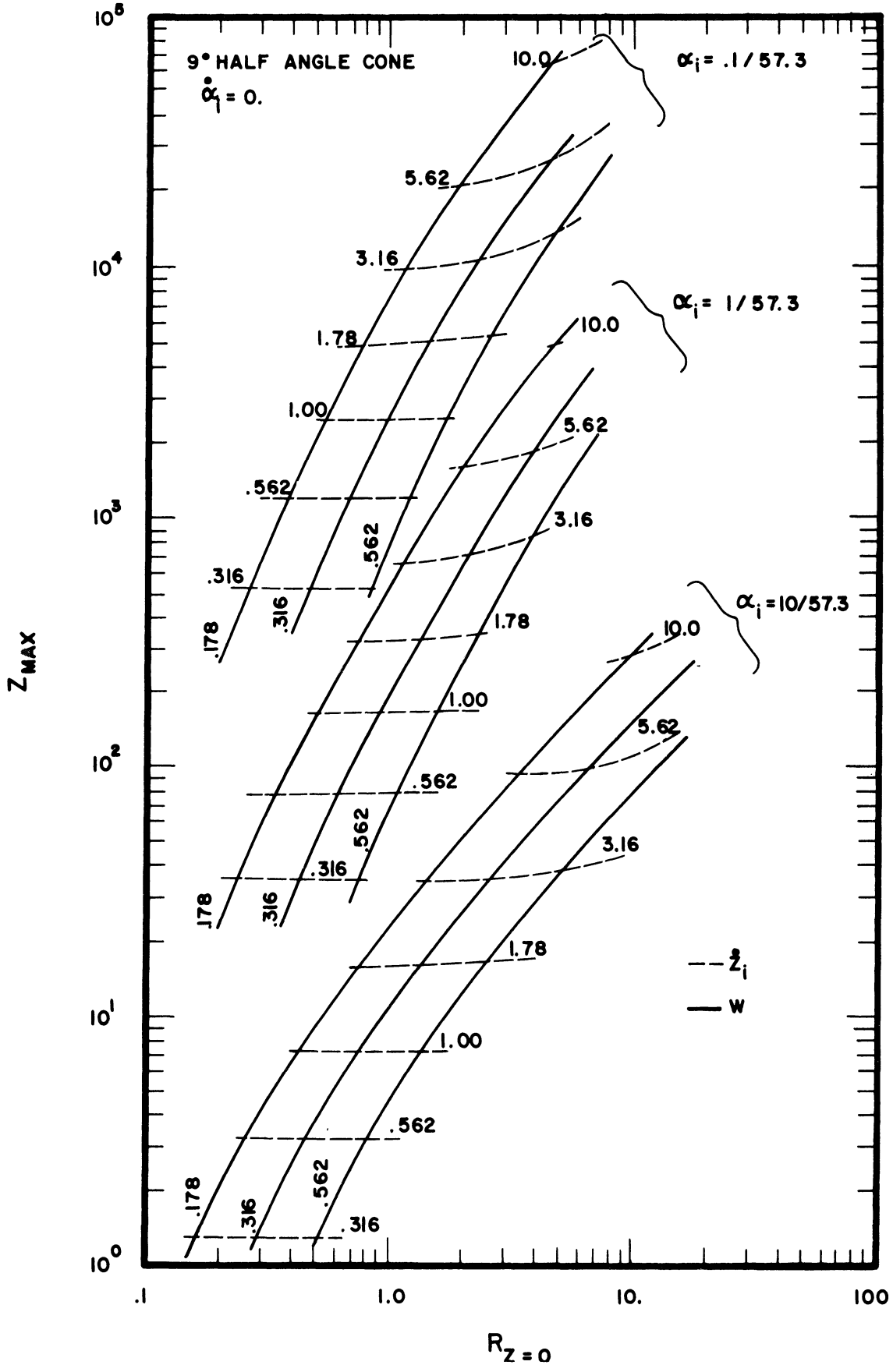

Figure 17. Nosetip performance chart.

6. REFERENCES

Cittadini, R. J., R. W. Simmons, and G. T. Poole, Theory and Data Processing for the Pitot Technique of Upper Atmosphere Measurement, University of Michigan Scientific Report 03632-1-S, April 1970.

Handy, P. O., Design of a Radioactive Ionization Gauge for Upper Atmosphere Measurements, University of Michigan Instrumentation Report 05776-1-I, February 1970.

Handy, P. O., Transforming the Ejectable Nosetip Equations of Motion for Efficient Solution, University of Michigan Internal Technical Note 03632-ITN, February 1971.

Neal, Jr., Luther, Aerodynamic Characteristics at a Mach Number of 6.77 of a 9° Cone Configuration, With and Without Spherical Afterbodies, At Angles of Attack Up to 180° With Various Degrees of Nose Blunting, Technical Note NASA TN D-1606, National Aeronautics and Space Administration, Washington, D.C., March 1963.

APPENDIX A. THEORY FOR NOSETIP MOTION

A.1. ANGULAR MOTION

The principle of moment of momentum for a rigid body expressed in a rotating coordinate system is

$$\frac{d\vec{H}}{dt} + \vec{\Omega} \times \vec{H} = \vec{M} \tag{1}$$

where

$\vec{\Omega}$ = coordinate system rotation rate with respect to an inertial frame of reference,
$\vec{H}$ = moment of momentum of the rigid body,
$\vec{M}$ = external moment applied to the body, and
t = instantaneous time.

For a rectangular coordinate system located at the center of mass as shown in Figure 18 below, the x, y, z axes are simply the principal axes of inertia of the symmetric nosetip.

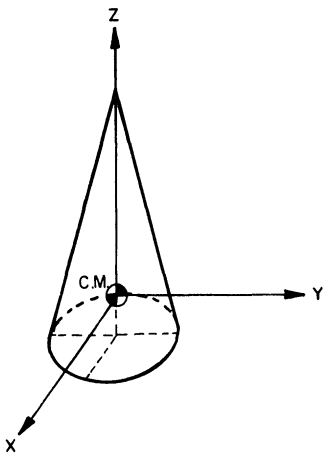

Figure 18. Coordinate system fixed at center of mass.

In component form, Equation (1) then becomes,

$$\frac{d(I_{xx}\omega_{x_n})}{dt} + (I_{zz}\omega_{z_n})\omega_{y_c} - (I_{yy}\omega_{y_n})\omega_{z_c} = M_x \tag{2}$$

$$\frac{d(I_{yy}\omega_{y})_n}{dt} + (I_{xx}\omega_x)_n \omega_{z_c} - (I_{zz}\omega_z)_n \omega_{x_c} = M_y \tag{3}$$

$$\frac{d(I_{zz}\omega_{z})_n}{dt} + (I_{yy}\omega_y)_n \omega_{z_c} - (I_{xx}\omega_x)_n \omega_{y_c} = M_z \tag{4}$$

where

subscripts n and c refer to the nosetip and coordinate systems respectively,

I_{xx}, I_{yy}, I_{zz} = principal moments of inertia of the nosetip, i.e., known constants,

$\omega_x, \omega_y, \omega_z$ = angular rotation rates about the x,y,z axes respectively,

M_x, M_y, M_z = components of the external moment.

The relation of the x,y,z coordinate system to an inertial frame of reference (x_o, y_o, z_o) used in this analysis is shown in Figure 19.

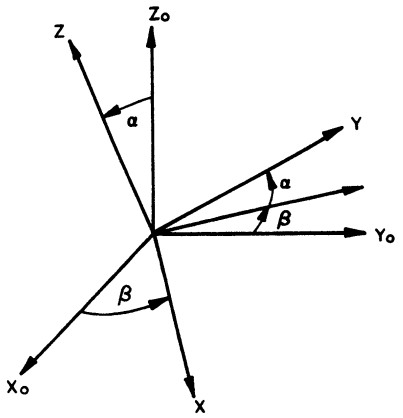

Figure 19. Inertial coordinate system.

The (x,y,z) coordinate system is derived by performing a rotation about the z_o axis through an angle β, followed by a rotation through an angle α about the newly formed x axis. The x,y,z coordinate system rotation rate is then

$$\vec{\Omega} = \frac{d\alpha}{dt}\hat{x} + \left(\frac{d\beta}{dt}\sin\alpha\right)\hat{y} + \left(\frac{d\beta}{dt}\cos\alpha\right)\hat{z} \tag{5}$$

and the nosetip rotation rate is

$$\vec{\omega}_n = \frac{d\alpha}{dt}\hat{x} + \left(\frac{d\beta}{dt}\sin\alpha\right)\hat{y} + \left(\frac{d\beta}{dt}\cos\alpha + \omega\right)\hat{z} \tag{6}$$

where

ω = rotation rate of the nosetip with respect to the rotating coordinate system (x,y,z).

Because of the definition of the coordinate system, the aerodynamic pitching moment will act about the x axis only. Hence,

$$M_y = M_z \equiv 0 \tag{7}$$

With Equations (5), (6), and (7) and noting $I_{yy} = I_{xx}$ because of symmetry, Equations (2), (3), and (4) become, respectively

$$I_{xx}\frac{d^2\alpha}{dt^2} + I_{zz}\left(\frac{d\beta}{dt}\cos\alpha + \omega\right)\frac{d\beta}{dt}\sin\alpha - I_{xx}\left(\frac{d\beta}{dt}\right)^2\sin\alpha\cos\alpha = M_x \tag{8}$$

$$I_{xx}\frac{d^2\beta}{dt^2}\sin\alpha + 2I_{xx}\frac{d\beta}{dt}\frac{d\alpha}{dt}\cos\alpha - I_{zz}\left(\frac{d\beta}{dt}\cos\alpha + \omega\right)\frac{d\alpha}{dt} = 0 \tag{9}$$

$$I_{zz}\frac{d}{dt}\left(\frac{d\beta}{dt}\cos\alpha + \omega\right) = 0 \tag{10}$$

Equations (8), (9), and (10) are the equations used in determining the angular orientation of the ejected nosetip. An expression for the aerodynamic pitching moment, M_x, is given later.

A.2. TRANSLATIONAL MOTION

Because of the definition of the rotating coordinate system used in this analysis, the aerodynamic normal and axial force components act only in the yz plane, i.e.,

$$\vec{F} = F_y\hat{y} + F_z\hat{z} \quad \text{with } F_x \equiv 0,$$

where

$\vec{F}$ = aerodynamic force encountered by the nosetip,

F_x, F_y, F_z = components of the aerodynamic force in the rotating coordinate system.

In the inertial frame of reference $\vec{F}$ is then expressed as

$$\vec{F} = F_y(-\cos\alpha\sin\beta)\hat{x}_o + F_y(\cos\alpha\cos\beta)\hat{y}_o + F_y\sin\alpha\hat{z}_o$$

$$+ F_z(\sin\alpha\sin\beta)\hat{x}_o + F_z(-\sin\alpha\cos\beta)\hat{y}_o + F_z\cos\alpha\hat{z}_o.$$

Thus, the equations for determining the translational motion of the nosetip are,

$$m\frac{dv_{x_o}}{dt} = -F_y\cos\alpha\sin\beta + F_z\sin\alpha\sin\beta, \tag{11}$$

$$m\frac{dv_{y_o}}{dt} = F_y\cos\alpha\cos\beta - F_z\sin\alpha\cos\beta, \text{ and} \tag{12}$$

$$m\frac{dv_{z_o}}{dt} = F_y\sin\alpha + F_z\cos\alpha, \tag{13}$$

where

m = mass of the nosetip, and

$v_{x_o}, v_{y_o}, v_{z_o}$ = velocity components in the inertial frame of reference.

An expression for F_y and F_z is determined in the next section.

A.3. AERODYNAMIC FORCE COMPONENTS AND PITCHING MOMENTS

A.3.1. Aerodynamic Coefficients

The coefficients used were taken directly from Neal (1963). His results were obtained from tests conducted with a 9 deg half angle cone at a Mach number of 6.77, a Reynolds number per inch of 135,000, and angles of attack from 0 deg to 180 deg. The moment reference was located 1.150·D forward of the base (where D is the base diameter of the cone).

Values of the aerodynamic coefficients are listed versus angle of attack in Table 1 where

C_M = pitching moment coefficient (P. Moment/$q_\infty SD$)

C_N = normal force coefficient (N. Force/$q_\infty S$)

C_A = axial force coefficient (A. Force/$q_\infty S$)

S = cone base area ($\pi D^2/4$), and

q_∞ = free stream dynamic pressure.

TABLE I

PITCHING MOMENT, NORMAL FORCE AND AXIAL FORCE COEFFICIENTS

α(deg)	C_M	C_N	C_A
0	0	0	.08
10	-.055	.35	.13
20	-.110	.73	.21
30	-.160	1.18	.27
40	-.227	1.62	.39
50	-.290	2.05	.46
60	-.330	2.38	.48
70	-.345	2.58	.49
80	-.355	2.63	.46
90	-.370	2.58	.42
100	-.390	2.38	.29
110	-.375	2.02	.02
120	-.340	1.62	- .39
130	-.255	1.20	- .82
140	-.130	.73	-1.21
150	-.078	.37	-1.46
160	-.055	.15	-1.63
170	-.025	.08	-1.72
180	0	0	-1.75

A.3.2. Force Components and Pitching Moments

From the definition of the coordinate system and the aerodynamic coefficients, the force components are simply,

$$F_y = -C_N q_\infty S \tag{14}$$

$$F_z = -C_A q_\infty S. \tag{15}$$

In Neal's tests the moment reference was located 1.150·D forward from the base of the cone. Thus, the expression for the aerodynamic pitching moment about the center of mass of an ejected nosetip is written as

$$M_x = (1.150 + C_M/C_N - \bar{x}) \cdot C_N q_\infty SD \tag{16}$$

where

$\bar{x}$·D = location of the center of mass from the cone base.

A.4. DYNAMIC PRESSURE CHANGES AND ROCKET VEHICLE DRAG

Because of vertical travel through the atmosphere the free stream dynamic pressure encountered by an ejected nosetip will change significantly. This effect becomes more important at higher ejection altitude. As can be seen in Figure 20 the dynamic pressure can be represented by the approximate expression

$$q_\infty(t) = q_{\infty_i} e^{-t/t_1}, \tag{17}$$

where

q_{∞_i} = dynamic pressure at the time of ejection,

t_i = appropriate time constant, and

t = instantaneous time.

The effect of aerodynamic drag on the rocket vehicle is also important, since the objective is a description of the trajectory of the ejected nosetip relative to the rocket. This effect can also be expressed in a simple form:

$$D(t) = D_i e^{-t/t_2} \tag{18}$$

where

D_i = rocket drag deceleration at time of ejection, and

t_2 = appropriate time constant.

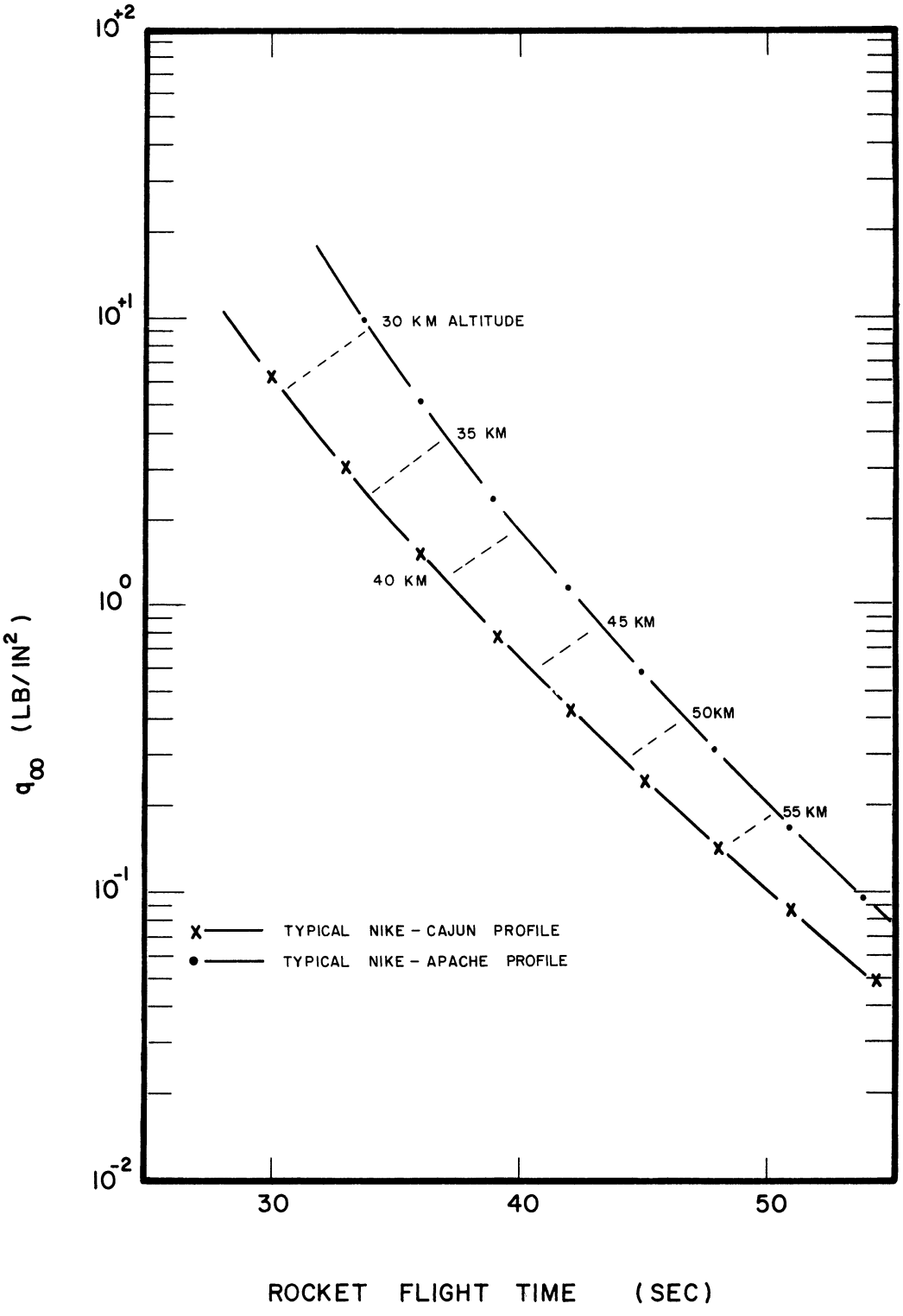

Figure 20. Free stream dynamic pressure versus rocket flight time.

APPENDIX B. NOSETIP MASS MEASUREMENTS

Both the weight and the center of mass location are carefully determined for each completely assembled nosetip. One particular nosetip weighed 3.44 lb with its center of mass located 3.950 in. forward from the cone base. In general, these measurements are typical of this nosetip design. However, both the weight and the center of mass location may be reestablished depending on the desired motion and possible trajectories of an ejected nosetip.

Since the spin is not a major influence of nosetip motion, the moment of inertia I_{zz} was roughly calculated based on estimated weight or mass distribution. For this, a radius of gyration of 1.1 in. was calculated and used.

However, the moment of inertia I_{xx} is an important parameter and was determined from experimental measurements rather than from calculations based on an estimated weight distribution. By allowing the nosetip to scillate like a pendulum, as shown schematically in Figure 21, the radius of gyration about the center of mass is related to the oscillation frequency by

$$K_{C.M.} = r\left[\frac{g}{4\pi^2 f^2 r} - 1\right]^{1/2}$$

where

r = distance between the pivot point and center of mass,
g = 32.16 ft/sec^2, and
f = oscillation frequency.

From the observed oscillation frequency and a measure of r, the radius of gyration for one typical nosetip about its center of mass was computed to be 3.06 in.

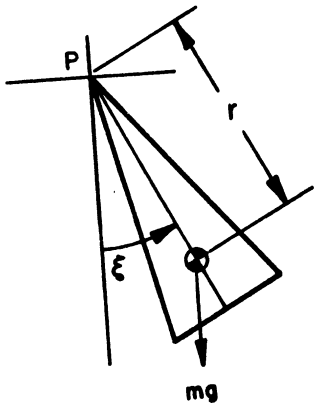

Figure 21. Determining the radius of gyration.

APPENDIX C. EJECTION TESTS

C.1. GROUND BASED TESTS

Nosetip ejection tests from ground based, payload simulated platforms were performed not only to gain confidence in the ejection scheme and in the structural design, but also to determine the behavior of the resulting motion. From both stationary and spinning platforms the piston actuators ejected complete nosetips to heights of approximately 27.5 ft. From the expression

$$v_i = (2gH)^{1/2}$$

where H = maximum height attained by the nosetip, and
$g = 32.16$ ft/sec^2,

an initial velocity, v_i, of 42 ft/sec was then computed. The initial ejection velocity is, of course, used in the determination of the trajectory of an ejected nosetip relative to a rocket.

From the nonspinning tests, tumble rates of less than 1 rad/sec and virtually straightforward and aligned ejection were also achieved. With the addition of spin (up to 12 cps) the ejected nosetip became completely stabilized and no tumble or coning was observed. During rocket flight, however, the expected minimal values of angle of attack and tumble rate initially encountered by the nosetip upon ejection are unknown due to the normally occurring variations in the rocket vehicle and, consequently, are considered as parameters in the nosetip motion analysis.

C.2. ENVIRONMENTAL EJECTION TEST

A thermal-vacuum spin ejection test was also performed in an environmental test chamber at Goddard Space Flight Center at the request of the newly formed Flight Readiness Review Board so that conditions encountered during rocket flight would be more closely simulated. In particular, the test was to determine if an external heat source, simulating aerodynamic heating, would cause the ejection mechanism to fail because of thermal seizure of lockup.

For the test setup, a nosetip was attached to a payload-shaped configuration which was mounted to a spin table centrally located inside the environmental test chamber. The spin table was tilted 3 deg so that the nosetip would land to one side in a pre-positioned net. An array of quartz filament

heaters was suspended about the nosetip to provide a uniform external heat source. To reduce air convection cooling the test chamber was evacuated to a pressure of 50 torr.

The test sequence of events is listed in Figure 22, which is also a profile plot of the temperature of a sensor located inside the nosetip. By agreement, the nosetip was to be ejected when this sensor indicated a temperature of 200°C. From the start, the test proceeded smoothly and was climaxed by a completely successful nosetip ejection at a spin rate of 6 rps.

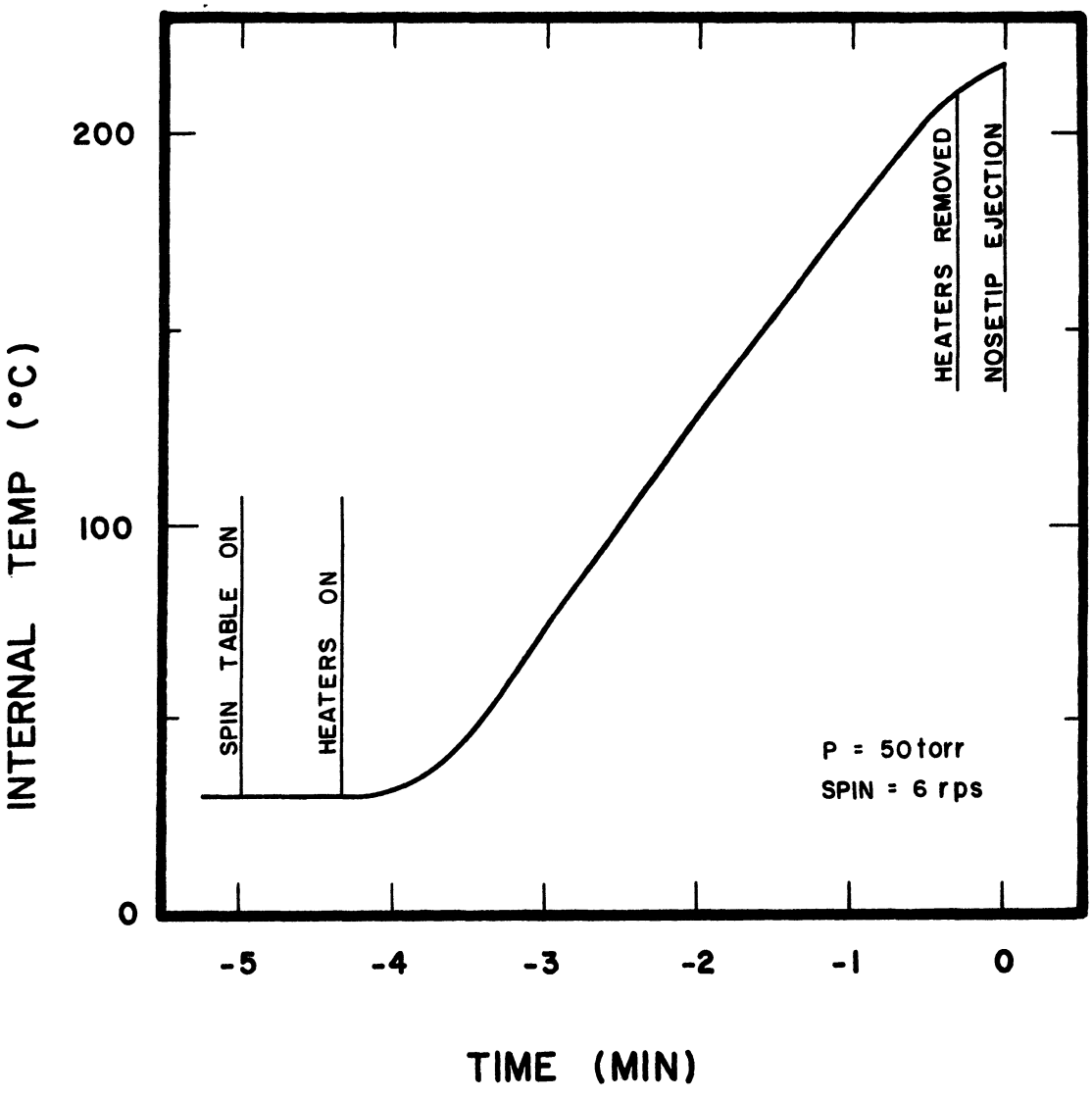

Figure 22. Temperature profile and sequence of events for thermal vacuum spin ejection test.